Optimization of single-stage x-ray laser coherence

Peter Amendt and Richard A. London
Lawrence Livermore National Laboratory, University of California, P. O. Box 808, Livermore, California 94550

Moshe Strauss
Physics Department, Nuclear Research Centre–Negev, Beer Sheva 84190, Israel
(Received 5 June 1992)

The effect of smoothly varying transverse gain and refraction profiles on x-ray laser coherence is analyzed by modally expanding the laser electric field within the paraxial approximation. Comparison with a square transverse profile reveals that smoothly varying profiles generally lead to a greatly reduced number of guided modes and a consequent improvement in transverse coherence length. However, the refractive defocusing responsible for enhanced coherence can also significantly degrade the coherent power of plasma x-ray lasers based on amplified spontaneous emission. A critical value of the Fresnel number is indicated, below which the coherent power rapidly decreases as refractive defocusing is increased. A parameter study of transverse coherence for current or planned x-ray laser experiments is provided. Comparison with ray-optics scaling laws for transverse coherence length and coherent power is made. An optimal coherent energy output of nearly 0.5 mJ in 100 psec is determined in Ni-like Ta at a wavelength of 45 Å for a saturated single-stage x-ray laser. A favorable comparison with coherent energy requirements for holographic imaging of biological samples is indicated.

PACS number(s): 42.50.Ar, 42.55.Vc, 42.60.Da, 52.25.Nr

I. INTRODUCTION

Current x-ray laser (XRL) designs rely on amplifying spontaneous emission in a high-temperature plasma [1]. An important issue in the study of XRLs is the degree of transverse spatial coherence necessary for holographic applications [2]. Longitudinal coherence appears to be satisfactory, but transverse coherence remains problematic and requires further optimization study.

Recently, London, Strauss, and Rosen have undertaken a study of transverse coherence based on a modal decomposition of the electric fields in an amplifying medium [3]. With this ansatz for the fields, the paraxial wave equation is transformed into two equations which separately govern the longitudinal and transverse behavior. The longitudinal equation describes the usual amplification from a distributed noise source, whereas the transverse equation describes the spectrum of eigenmodes which determines the possible transverse profiles of intensity and coherence.

The above mathematical characterization for the fields has formed the basis in the literature for the predicted phenomenon of "excess noise" in an amplifying medium [4]. In particular, the inherent non-self-adjoint property of the transverse equation in a general amplifying medium presumably allows for the possibility that loosely guided or bound transverse eigenmodes may dominate the profiles at large transverse distances from the lasing medium. Such a prospect has serious implications since the predicted coherence and intensity profiles will be overly sensitive to the precise gain profile used, which we argue cannot be physical.

Originally the modal approach to understanding XRL phenomena was confined to the bound mode or discrete portion of the transverse eigenmode spectrum. For sufficiently large values of gain-length product this restricted analysis can obtain accurate transverse profiles of intensity and coherence. Unfortunately, most gain-length products achieved in the present generation of amplified-spontaneous-emission XRL experiments are not sufficiently large to justify use of this truncated approach.

More recently, we have reexamined the modal approach by appending the continuum or free modes to the bound-mode portion of the transverse spectrum for the particular example of transverse square gain and density profiles [5]. The primary motivation for including the continuum is that by virtue of the nonorthogonality and assumed completeness of the eigenmodes, sufficient cancellation from cross terms in the expression for the modal intensity may occur and possibly eliminate to a large extent the excess-noise phenomenon. It was found that for small and moderately large gain-length products the anomalously large intensities associated with loosely bound transverse modes are significantly reduced by the inclusion of neighboring free eigenmodes. This feature has the twofold effect of greatly reducing the level of excess noise and of removing the source of undue sensitivity of previous modal modeling to the exact value of the gain parameter adopted.

Although we have previously addressed some fundamental problems arising in a general XRL environment, the degree of transverse coherence has not been sufficiently characterized. In particular, the square gain and density profiles explored in that analysis were intended primarily for analytic ease and conceptual clarity. What remains to be shown is whether the modal intensity cancellation persists as effectively for rounded profiles which presumably provide for increased transverse

coherence through refractive defocusing effects. In this paper we continue our analysis of modal XRL coherence by considering some consequences of rounded gain and density profiles. The large degree of excess noise arising from the few bound modes for a rounded transverse profile requires the inclusion of free modes in the analysis. We compare our transverse coherence profiles with those produced by square profiles and show that refractive defocusing greatly enhances the coherence length as expected. However, the on-axis intensity may be seriously compromised by strong refraction. We find that there is a critical value of the Fresnel number below which the coherent power decreases as refraction is increased. Below this critical value the coherence length continues to improve with refraction, but the coherent power falls rapidly and increased refraction becomes no longer beneficial. This suggests that we always operate slightly above this critical Fresnel number. However, the output power of such a small Fresnel number laser is limited by gain saturation. We consider saturation effects in the vicinity of this critical value of the Fresnel number and show that the optimum coherent energy output in Ni-like Ta at 45 Å in 100 psec is nearly 0.5 mJ. For holographic imaging of live biological structures at a useful resolution of nearly 300 Å, this optimum output compares with calculated requirements for coherent energy generation [2]. However, possible nonoptimal performance of single-stage x-ray lasers in holographic studies may reinforce consideration of multipass or multi-stage amplifiers with spatial filtering.

The paper is organized as follows. Section II introduces notation and summarizes the modal approach; Sec. III investigates transverse coherence in a finite geometry starting from the eigenmodes of a square profile; Sec. IV analyzes coherence in an unbounded geometry as a means of avoiding any possible sensitivity of our results on boundary phenomena; in Sec. V scaling laws for transverse coherence length and power based on ray optics are developed and compared with the modal predictions; and finally in Sec. VI a summary of our results is presented.

II. MODAL PRELIMINARIES

Our starting point for the modal analysis is the paraxial equation in one transverse dimension for the slowly varying wave electric-field amplitude E_ω with frequency component ω [3,5]:

$$\left[\frac{1}{k}\partial_{xx}^2 - 2i\partial_z - h(x) + ig(x)\right]E_\omega(x,z) = -4\pi k P_{\rm sp}(x,z) , \quad (1)$$

where k is the free-space longitudinal (or parallel to z axis) wave vector, $h=\omega_{pe}^2(x)/kc^2$, ω_{pe} is the electron plasma frequency, $g(x)$ is the atomic gain of the medium, and $P_{\rm sp}$ is the random (in x and z) spontaneous atomic polarization. After writing $E_\omega(x,z)=\sum_n c_n(z)u_n(x)$ we find a transverse mode equation

$$\{\partial_{xx}^2 - F_e[\eta h(x) - ig(x)]\}u_n(x) = -E_n u_n(x) , \quad (2)$$

and a longitudinal transfer equation

$$\sum_n \left[u_n \partial_z c_n - \frac{i}{2}E_n c_n u_n\right] = -iP_{\rm sp} , \quad (3)$$

where $F_e=kg_0a^2$ is an effective Fresnel number, a is a lasing medium (horizontal) transverse scale length, E_n is the eigenvalue, $x\to xa$, $z\to zka^2$, $P_{\rm sp}\to P_{\rm sp}/2\pi(ka)^2$, $\eta=h_0/g_0$ is a normalized density parameter, and $h\to h/h_0$ and $g\to g/g_0$ are normalized transverse profiles. Since Eq. (2) is non-self-adjoint, the eigenvalues are generally nonreal and the eigenfunctions are *biorthonormal:* $\int u_n u_m dx=\delta_{nm}$ $(\neq\int u_n u_m^* dx)$. This feature specifically gives rise to the problem of excess noise, where loosely bound modes may dominate the electric-field intensity $c\langle|E_\omega|^2\rangle/8\pi$ at large transverse distance $(x\gg 1)$. We have previously shown for hard-edged square gain and density profiles that free modes $(\lim_{x\to\infty}|u_n|>0)$ contained in the spectrum of Eq. (2) tend to compensate for excess noise arising from bound modes $(\lim_{x\to\infty}u_{n'}=0)$ which are marginally bound [5]. However, the case of a hard-edged profile is not a realistic feature of plasma XRL's. We consider an example of a more realistic smooth profile below.

Using Eq. (3) and assuming that the spontaneous emission is δ-function correlated in space [3,5], we may write for the electric-field correlation function

$$\langle E_\omega(\mathbf{r}_1)E_\omega^*(\mathbf{r}_2)\rangle = \sum_{n,m}\langle c_n(z)c_m^*(z)\rangle u_n(x_1)u_m^*(x_2) = C_1\sum_{n,m}(e^{iz(E_n-E_m^*)/2}-1)\times B_{nm}u_n(x_1)u_m^*(x_2) , \quad (4)$$

where $B_{nm}=\int u_n u_m^* dx$ is the overlap integral, $C_1=2(\pi/\ln 2)^{1/2}(N_2/\Delta N)\hbar k\Delta\omega_D/(ab)$ [6], N_2 is the upper-level population with degeneracy g_2, and the fractional population inversion factor $\Delta N/N_2=[1-g_2N_1/g_1N_2]$ is assumed constant. Additionally, c is the speed of light, $\Delta\omega_D$ is the full width at half maximum atomic linewidth for a Doppler profile, and b is a lasing medium (vertical) transverse scale length. We define the *coherence function* as the absolute value of the complex coherence factor [7]

$$\mu(x_1,x_2;z)=\left|\frac{\langle E_\omega(x_1,z)E_\omega^*(x_2,z)\rangle}{[\langle E_\omega(x_1,z)E_\omega^*(x_1,z)\rangle]^{1/2}[\langle E_\omega(x_2,z)E_\omega^*(x_2,z)\rangle]^{1/2}}\right| . \quad (5)$$

For example, μ equals the fringe visibility in a two slit interferometer with equal slit intensity, i.e., $\langle E_\omega(x_1,z)E_\omega^*(x_1,z)\rangle=\langle E_\omega(x_2,z)E_\omega^*(x_2,z)\rangle$.

For partially coherent sources the coherence function is near unity for very small transverse separations $|x_2-x_1|$ and drops to zero for large separations. A coherence length x_c is defined as the value of $|x_2-x_1|$ at which μ has dropped from unity to some characteristic value. To be more precise, we choose this characteristic value of μ based on the conventional example of an incoherent disk radiator. For a one-dimensional incoherent source of half-width a the coherence function at a distance L has been calculated from the van Cittert-Zernike theorem [7–9]: $\mu=\sin(\rho)/\rho$, where $\rho=ka|x_2-x_1|/L$. According to the usual convention, we define a (normalized) coherence length ($x_c/a\rightarrow x_c$) as the distance $|x_2-x_1|$ over which μ drops from unity (at $x=0$) to $\sin(1)\approx 0.8415$. In the case of the incoherent disk source $x_c=L/ka^2\equiv 1/F_x$, where F_x is the Fresnel number in the x direction.

The choice of a one-dimensional transverse scale length a requires further elaboration. We associate a with the scale length of the (horizontally) exploding foil plasma at the peak of the ionizing laser pulse (or near peak gain) for the following reason. In the horizontal direction the electron density appears to be well approximated by a $\mathrm{sech}^2(x)$ profile, but the profile in the vertical transverse direction (or across the line focus) more closely resembles a square profile. By comparing square and smooth profiles, we expect that refractive defocusing should greatly improve transverse coherence for the latter class of profile. An important question that arises is when does the horizontal transverse dimension predominantly determine the degree of horizontal coherence which appears to benefit most from refractive defocusing. Certainly, this occurs before the foil plasma has expanded appreciably since the resulting coherence pattern must resemble the coherent output from a thin (vertical) slit which varies only with slit thickness. Later in time as the plasma continues to expand horizontally, the vertical transverse dimension will begin to have an important effect on horizontal coherence, and a two-dimensional transverse treatment is preferred. Here, we continue with a one-dimensional transverse analysis for simplicity, bearing in mind the possible importance of vertical effects on horizontal coherence at later times.

III. MODAL STUDY WITH REFRACTION: FINITE GEOMETRY

In our previous study with square transverse profiles, we concluded that the inclusion of free modes (or standing waves) was essential to reliably model coherence and intensity for moderate values of gain-length product ($g_0L<10$). To introduce and define the free modes used in the analysis, we imposed reflecting boundaries at $x=\pm A$ and chose A substantially larger than a laser transverse dimension in order to minimize the dependence of our results on the actual location of the boundary. In this section we follow this same procedure for a smoothly varying transverse profile. We choose to concentrate on a $\mathrm{sech}^2(x)$ profile instead of the parabolic profile considered in detail in Ref. [3] because it possesses both the physically realistic properties of going to zero smoothly as $|x|\rightarrow\infty$ and of being rounded near $x=0$. In addition, this profile is mathematically convenient because (i) the bound-mode eigenvalues are analytically known in the case of an unbounded geometry, and (ii) the integrated area under $g(x)$ coincides with the square profile. The eigenvalues are simply [10]

$$E_n=-\{\tfrac{1}{2}[1+4iF_e(1+i\eta)]^{1/2}-(n+\tfrac{1}{2})\}^2\ ,\qquad n=0,1,2,\ldots\ , \tag{6}$$

while the associated transverse eigenfunctions take the form of confluent hypergeometric functions as $A\rightarrow\infty$.

The general requirement for a bound mode is that $\lim_{A\rightarrow\infty}\mathrm{Im}(E_n)<0$, leading to only several bound modes at most for current XRL experimental parameters (see Table I). By contrast, the number of modes n_g in a hard-edged (square profile) laser scales as [3] $2F_e/\{\pi\ln[F_e/(1+\eta)]\}$, giving typically several hundred bound modes. Clearly, the coherence length would be far greater for a smooth profile than for a square profile, if we were to consider only the bound-mode contribution. The key question becomes to what extent does the inclusion of free modes [$\lim_{A\rightarrow\infty}\mathrm{Im}(E_n)=0$] affect this conclusion.

To consider this question, we first show how the free modes compensate for anomalous intensities arising from loosely bound modes as previously shown for the square profile case [5]. The bound and free modes are obtained by numerically relaxing the eigenmodes of Eq. (2) for a square profile into the corresponding modes of the $\mathrm{sech}^2(x)$ profile and by using a reflecting boundary condition at $x=A$. A useful method to this end is to first relax the square profile into a $\mathrm{sech}^2(x)$ profile as follows: $h(x),g(x)\rightarrow(1-\epsilon)f(x,\epsilon)+\epsilon\,\mathrm{sech}^2(x)$, where $\epsilon\rightarrow 1$ and

$$f(x,\epsilon)=\begin{cases}0, & |x|>1+\epsilon\\ \sin^2\left[\dfrac{\pi(|x|-1-\epsilon)}{4\epsilon}\right], & 1-\epsilon<|x|<1+\epsilon\\ 1, & |x|<1-\epsilon\ .\end{cases} \tag{7}$$

In Fig. 1 we display several examples of the transformation function $f(x,\epsilon)$ as ϵ is varied from zero (square profile) to unity (smooth profile). We then solve (by the shooting method) the transverse eigenvalue Eq. (2) at each incremental step in ϵ using the eigenvalue for the

TABLE I. XRL parameters for current coherence experiments at Lawrence Livermore National Laboratory. For Ne-like Se the quoted gain-length product is the saturation value [27], which is less than the maximum measured value of $g_0L=26$.

XRL	λ (Å)	n_e (cm^{-3})	a [μm]	F_e	η	g_0L
Ne-like Se	206	3.5×10^{20}	200	4880	101	16
Ni-like Ta	45	2.0×10^{21}	75	2356	168	9

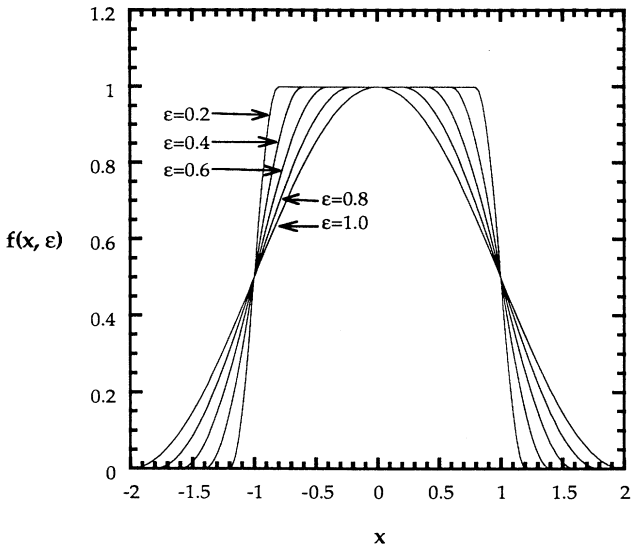

FIG. 1. Shown are plots of Eq. (7) for several values of ϵ which describe the transformation from a square profile ($\epsilon=0$) to a smooth profile ($\epsilon=1$) with continuous derivative everywhere.

previous ϵ as a guess. As $\epsilon\rightarrow 1$ both the free and bound eigenfunctions of the $\text{sech}^2(x)$ profile are successively obtained. Figure 2(a) shows how rapidly all but one of the first seven squarelike bound modes ($\epsilon=0$) become free modes as ϵ is increased from zero to one. As ϵ approaches unity, the free modes are found to lie in a distinct band [in $\text{Im}(E_n)$] well removed from the lone remaining bound mode. For larger A, the distinction between the two classes of modes becomes unambiguous since the imaginary part of E_n for the free modes scales generally as $1/A$, whereas the imaginary part of E_n for the bound modes is independent of A. In Fig. 2(b) we show the point (or bound mode) and continuum (or free-mode) spectra for both square and $\text{sech}^2(x)$ profiles in the complex E plane. Although the imaginary part of E_n for free modes vanishes as $1/A$, the *phase-space* density of free modes increases with A. This property means that the resonance of free modes with a neighboring bound mode is relatively independent of A and is a persistent feature even as $A\rightarrow\infty$. We note the absence of continuum resonances beyond the one (even-parity) bound mode for the $\text{sech}^2(x)$ profile; such resonances effectively act as loosely bound modes in the case of the square profile [5]. The numerous continuum resonances characteristic of the square profile have coalesced to give a single broad resonance situated just below the bound mode. This generic feature of the smooth profile simplifies the analysis: relatively more free states behave as high or nearly orthogonal modes which happen to depend only weakly on the details of the gain and density profiles.

Figures 3(a)–3(b) display the compensated intensity for one loosely bound mode compared to the uncompensated or "bare" intensity, using Eq. (4). We note how the bound-mode intensity dramatically cancels beyond $x\approx\pm 2$ for the compensated case, while in the absence of resonant free modes a considerable surplus of energy resides outside the lasing medium ($|x|\geq 1$). This example illustrates the excess-noise phenomenon for a smooth profile, but with a significant degree of reduction occurring due to cross correlations between neighboring [in

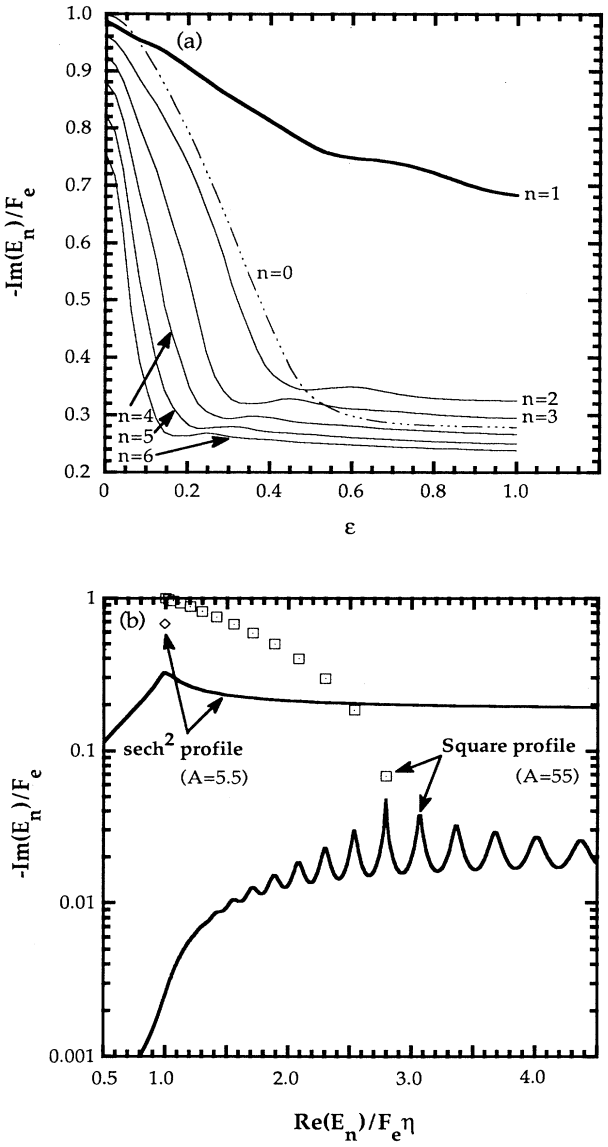

FIG. 2. (a) Imaginary part of the eigenvalue for the first seven even-parity bound eigenfunctions of the square profile ($\epsilon=0$) as the parameter ϵ [cf. Eq. (6)] is increased to unity. At $\epsilon=1$ a clear separation between the one remaining bound mode (heavy solid line) of the $\text{sech}^2(x)$ profile and a collection of free eigenfunctions of Eq. (2) is evident. Note in addition how the second bound eigenfunction of the square profile is transformed into the lone bound mode of the $\text{sech}^2(x)$ profile for this particular case. (b) Spectrum of bound and free eigenvalues for both the square and $\text{sech}^2(x)$ profiles. In both figures $F_e=100$ and $\eta=10$. The larger value of outer boundary location or A used in the square profile in (b) is for the purpose of resolving the continuum resonances.

$\mathrm{Re}(E_n)$] free modes and the one marginally bound mode. For larger gain-length product the intensity compensation from free modes is reduced to the point that the total intensity becomes dominated by the bound-mode intensity. In this case, the excess noise is not further reduced by cross correlations but persists as previously predicted [4,5].

In Fig. 4 we compare coherence profiles for the square and $\mathrm{sech}^2(x)$ profiles. The improved coherence for the $\mathrm{sech}^2(x)$ profile is due mainly to the fewer number of bound modes in the system. This trend can be understood from either a geometrical optics or modal viewpoint. In the former, the loss of modes is due to refractive defocusing, which bends rays away from the lasing medium, whereas the latter attributes the improved coherence to an effectively reduced region of maximum gain which limits the number of high-gain transverse modes possible. In general, refraction contributes significantly in discarding many of the bound modes responsible for degraded transverse coherence [3].

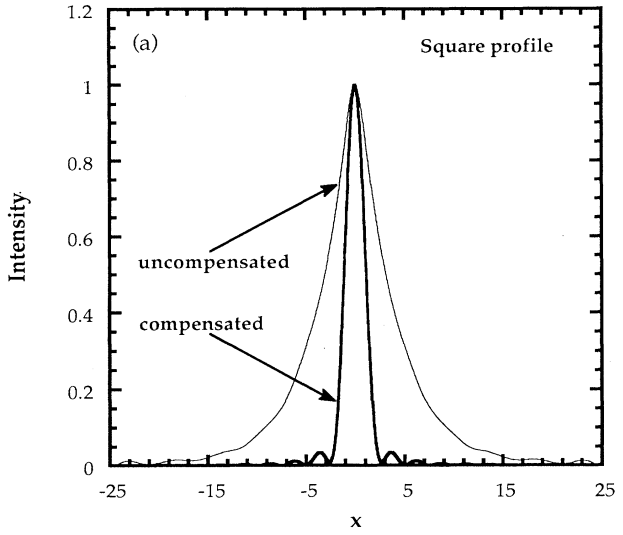

FIG. 3. Shown are the compensated (heavy solid line) and uncompensated (solid line) normalized intensity profiles for the square (a) and $\mathrm{sech}^2(x)$ (b) profiles. In both figures, $F_e=0.5$, $\eta=0$, $g_0L=0.1$, and $A=25$.

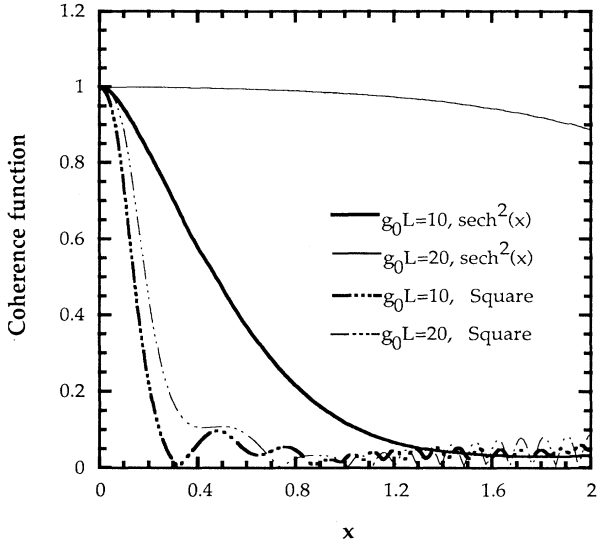

FIG. 4. Shown are the coherence functions vs normalized transverse position x for the square (dotted-dash line) and $\mathrm{sech}^2(x)$ (solid line) profiles for two values of gain-length product g_0L with $F_e=100$, $\eta=10$, and $A=5.5$.

Our strategy of numerically evolving each square profile mode (bound and free) directly into an eigenmode of the $\mathrm{sech}^2(x)$ profile is time consuming and not well suited for a parameter study of coherence in current XRL experiments. Moreover, our finite-boundary procedure will bear some dependence on both the position and nature of the boundary which we seek to avoid. In the next section we develop a method for simplifying the role of the continuum on XRL coherence and eliminating any possible boundary effects in our analysis.

IV. MODAL STUDY WITH REFRACTION: UNBOUNDED GEOMETRY

A. Algorithm for $A \to \infty$

Rather than deriving detailed features of the free-mode portion of the spectrum which are associated with a bounded geometry ($A < \infty$), we aim in this section to extract only those necessary features of the continuum which have a bearing on transverse coherence. Our starting point is Eq. (2), where the reflecting boundary is moved to infinity ($A \to \infty$). Bear in mind that our modal formulation with a reflecting boundary condition is identified with standing waves and not traveling waves emanating from a localized source region. Both descriptions are mathematically equivalent as $A \to \infty$ for a complete set of basis functions. We assume that a complete set consisting of bound modes and standing waves is at hand in the modal formulation for a refracting medium (see Ref. [5] for a detailed discussion of spectral com-

pleteness for a squarelike gain medium). We define an intermediate boundary at $x=A_i$ such that both $g(x)$ and $h(x)$ are much less than unity beyond A_i. We assume that the continuum solutions can be obtained numerically in the central region ($x \le A_i$) by treating the eigenvalue E_n as a continuous variable E. In this way, $u_E(A_i)$ and $(d/dx)u_E(A_i)$ are readily gotten by integrating Eq. (2) from $x=0$. In the outer region ($x > A_i$) the plane-wave solutions to Eq. (2) are used:

$$u_E(x)=D_E e^{i\sqrt{E}x}+H_E e^{-i\sqrt{E}x} . \tag{8}$$

From the continuity requirement on u_E and $u'_E=du_E/dx$ at $x=A_i$, we find

$$D_E=\frac{e^{-i\sqrt{E}A_i}}{2}\left[u_E(A_i)-i\frac{u'_E(A_i)}{\sqrt{E}}\right] , \tag{9a}$$

$$H_E=\frac{e^{i\sqrt{E}A_i}}{2}\left[u_E(A_i)+i\frac{u'_E(A_i)}{\sqrt{E}}\right] . \tag{9b}$$

Thus, $u_E(x)$ is determined for all x provided $u_E(x)$ is known for $x \le A_i$.

A dispersion relation follows from Eqs. (8), (9a), and (9b) by imposing a reflecting boundary condition on the transverse field, i.e., $u_E(A)=0$,

$$u_E(A_i)+\frac{u'_E(A_i)}{\sqrt{E}}\tan[\sqrt{E}(A-A_i)]=0 . \tag{10}$$

In the limit as $A\to\infty$, it is straightforward to show from Eq. (10) for the case of free modes not in resonance with a bound mode that $\mathrm{Re}(E^{1/2})\approx -m\pi/A$ and $\mathrm{Im}(E^{1/2})\approx F_e/A$, where m is a large integer and $\mathrm{Im}(E^{1/2})\ll\mathrm{Re}(E^{1/2})$ is used [11]. Thus, the free-mode dispersion relation simplifies to the usual form for a free-space wave in a large box when the "energy" far exceeds the "potential" barrier.

The normalization of the free states is determined by the requirement

$$\int_0^A v_E^2(x)dx=1 ,$$

where $v_E=N_E u_E$ and N_E is the normalization constant. Using Eq. (8) and taking A very large yields $N_E=(2D_E H_E A)^{-1/2}$, which has the familiar form of a box normalization for standing waves. The normalization for the bound modes N_n is defined similarly, although a numerical evaluation is required.

Having described the essential features of the continuum, we now proceed to evaluate Eq. (4) for the electric-field correlation function:

$$\langle E_\omega(x_1,z)E^*_\omega(x_2,z)\rangle = C_1\left\{\sum_{n,m}B_{n,m}u_n(x_1)u^*_m(x_2)(e^{iz(E_n-E^*_m)/2}-1)+\sum_{E,E'}B_{E,E'}u_E(x_1)u^*_{E'}(x_2)(e^{iz(E-E'^*)/2}-1)\right.$$
$$\left.+\sum_{n,E}B_{n,E}u_n(x_1)u^*_E(x_2)(e^{iz(E_n-E^*)/2}-1)+\sum_{E,n}B_{E,n}u_E(x_1)u^*_n(x_2)(e^{iz(E-E^*_n)/2}-1)\right\} , \tag{11}$$

where the first expression on the right-hand side is the bound-bound (b-b) contribution, the second term is the free-free (f-f) portion, and the last two terms are the bound-free (b-f) and free-bound (f-b) components, respectively. Upon defining $\beta_E=E^{1/2}$ and using

$$\frac{1}{A}\sum_E \to \frac{1}{\pi}\int_{-\beta_{\max}}^0 d\beta_E \tag{12}$$

in the limit as $A\to\infty$, cf. Eq. (10), we may rewrite Eq. (11) as follows:

$$\langle E_\omega(x_1,z)E^*_\omega(x_2,z)\rangle = C_1\left\{\sum_{n,m}F_{n,m}N_n^2N_m^{2*}u_n(x_1)u^*_m(x_2)\frac{2(e^{iz(E_n-E^*_m)/2}-1)}{i(E_n-E^*_m)}\right.$$
$$+\frac{1}{2\pi^2}\int_{-\beta_{\max}}^0\int_{-\beta_{\max}}^0 d\beta\,d\beta' F_{\beta,\beta'}\frac{(e^{iz(\beta^2-\beta'^2)/2}-1)}{i(\beta^2-\beta'^2)}\frac{u_\beta(x_1)u^*_{\beta'}(x_2)}{D_{E(\beta)}H_{E(\beta)}(D_{E(\beta')}H_{E(\beta')})^*}$$
$$+\frac{1}{\pi}\sum_n N_n^2\int_{-\beta_{\max}}^0 d\beta F_{n,\beta}\frac{(e^{iz(\beta_n^2-\beta^2)/2}-1)}{i(\beta_n^2-\beta^2)}\frac{u_n(x_1)u^*_\beta(x_2)}{(D_{E(\beta)}H_{E(\beta)})^*}$$
$$\left.+\frac{1}{\pi}\sum_n N_n^{2*}\int_{-\beta_{\max}}^0 d\beta F_{\beta,n}\frac{(e^{iz(\beta^2-\beta_n^{2*})/2}-1)}{i(\beta^2-\beta_n^{2*})}\frac{u_\beta(x_1)u^*_n(x_2)}{D_{E(\beta)}H_{E(\beta)}}\right\} , \tag{13}$$

where

$$F_{\alpha,\alpha'}=\int_0^{A_i} dx\, g(x)u_\alpha(x)u^*_{\alpha'}(x), \quad \alpha,\alpha'=n \text{ or } \beta . \tag{14}$$

Two important features stand out in Eq. (13). First, the free state normalization factor $1/(D_{\beta(E)}H_{\beta(E)})$ is seen from Eqs. (9a) and (9b) to have a pole near the bound-mode dispersion relation $v_n(A_i)=iv'_n(A_i)/\beta_n$, which is obtained from Eq. (10) by assuming (by definition of a bound mode) that $\mathrm{Im}(E_n)<0$ in the limit as $A\to\infty$. This resonance phenomenon becomes particularly problematic for high effective Fresnel numbers F_e where the resonance is quite sharp and thus difficult to treat numerically. The evaluation of Eq. (13) proceeds by first solving Eq. (2) for the eigenfunctions up to $x=A_i$ and then performing the β integrations with sufficiently small grid spacing in order to satisfactorily resolve the continuum resonances. An additional caveat is that A_i must be taken sufficiently large so that spurious structure on each continuum resonance can be avoided. This additional structure closely resembles near-field Fresnel diffraction ripples and results from effectively truncating the gain and refraction profiles for too small a choice of A_i. This phenomenon generally occurs for effective Fresnel numbers exceeding several hundred and is ameliorated by increased density parameter η or choosing larger A_i.

B. Spectral cutoff

To choose a value of $\beta_{\max}$ it is helpful to bear in mind that for large β, the free modes approximate standing plane waves with transverse wave numbers also equal to β. Thus, their propagation angle relative to the laser axis is characterized by $\tan^{-1}(\beta/k)$. The natural choice of $\beta_{\max}$ is that at which the propagation angle of the wave becomes large ($\approx\frac{1}{2}$ rad). Such a choice naturally leads to a complete description of all radiation consistent with the paraxial approximation made at the beginning of the analysis. However, such a large choice for $\beta_{\max}$ makes the numerical evaluation of Eq. (13) difficult.

There are two practical considerations which could lead to a choice of a more manageable (or smaller) value of $\beta_{\max}$. The first is based on the experimental setup for viewing or utilizing the laser. Instruments such as spectrometers, beam pattern cameras, or interferometers viewing a laser usually have a small acceptance angle, typically 1–50 mrad. To calculate what such an instrument would measure, we need to keep only eigenfunctions whose corresponding propagation angles are less than the instrument acceptance angle. Another more general choice for $\beta_{\max}$ is to consider the expected angular width of the radiation pattern emitted by the laser. For example, a constant gain and density XRL with large Fresnel number produces a beam of characteristic angular width equal to the laser width over its length ($\approx 2a/L$). For the more realistic case of strong refraction, the width of the radiation pattern is characterized by a refraction angle $\phi_R=\omega_{pe}/\omega=(F_e\eta)^{1/2}/(ka)$ [12].

The refraction angle ϕ_R is a key quantity in optical waveguide theory and in geometrical optics treatments of XRL propagation; it is defined as the exit angle of a refracting ray which starts out along the axis of symmetry of a long XRL with infinitesimally small angle relative to the z axis. In fact, we have determined by analyzing the modal wave spectrum through Fig. 2(b) that the continuum resonance coincident with the bound modes occurs very close to the transverse wave number corresponding to a refraction angle. This strong correspondence between refraction angle and modal resonance suggests that we identify the maximum transverse wave number with the exit angle $\phi_{\max}$ (times k) of the single ray that traverses the refracting medium from corner ($x=1$, $z=0$) to corner ($x=1$, $z=L$) as shown in Fig. 5, thereby assuring that the resonances occurring in Eq. (13) are always contained within the range of the β integration. In more physical terms, we choose to retain only those wave functions corresponding to rays which principally traverse the region of gain guiding along the entire length of the laser, taking into account their refractive properties through ϕ_R. This prescription is well suited for our purposes at hand: a strongly refracting environment with a moderate to large gain-length product in which the angular distribution indeed sharply decreases beyond a refraction angle. For the special case of a nonrefracting (geometric) medium or a refracting medium with small gain length, extended tails on the angular distribution may give a large contribution to the radiation intensity in the near field, i.e., near the end of the laser. For such cases it would be desirable to impose instead a cutoff based on the angular acceptance of the detector.

Because the $\mathrm{sech}^2(x)$ profile goes to zero only when $x\to\infty$, the above prescription requires modification to ensure that the modal resonance is always contained within the range of β integration in Eq. (13). For example, a ray which starts out along the axis of symmetry with an infinitesimally small opening angle "exits" the medium at $x=x_0$ with angle *less* than ϕ_R by the factor $\tanh(x_0)$. As mentioned above, we choose to include in practice only those eigenfunctions that correspond to rays which are contained within $x_0=\pm 1$ along the whole length of the laser. For the cases of strong refraction we have in mind, $\phi_{\max}$ turns out to be only slightly larger than $\phi_R\tanh(1)$, which means that our adopted cutoff for β as graphically illustrated in Fig. 5 will fall well short of the modal resonance at $\beta=(F_e\eta)^{1/2}/a$. To circumvent this occurrence we choose to make the replacement $\phi_{\max}\to\phi_{\max}/\tanh(1)$, which effectively increases the range of β integration in Eq. (13). We emphasize that this feature is only an artifact of the infinite transverse extent of the $\mathrm{sech}^2(x)$ profile unlike the case of a truncated or localized profile considered previously, i.e., a hard-edged square profile [5].

C. Weakly bound modes and excess noise

The modal resonances become particularly sharp as a new bound mode is formed which occurs when either F_e is increased or η is reduced. From Eq. (6) we can specify precisely when this occurs ($F_e,\eta\gg 1$):

$$F_e=(2n+1)^2\eta, \quad n=0,1,2,\ldots . \tag{15}$$

For F_e less than η, no bound modes are present so that

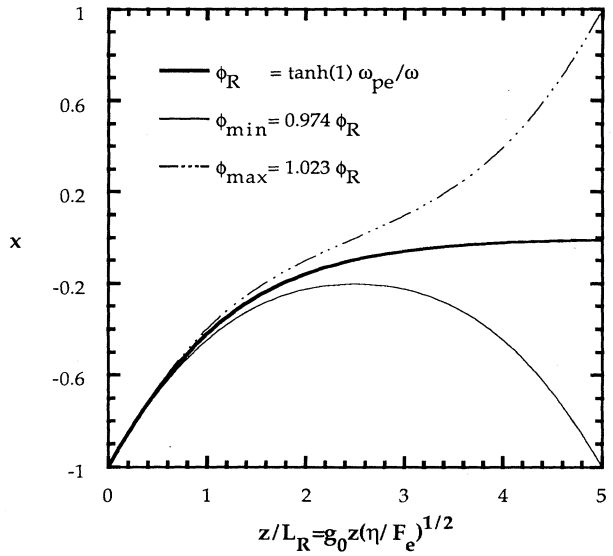

FIG. 5. Shown are the minimal (solid line) and maximal (dotted-dash line) ray trajectories and indicated respective opening angles $\phi_{\min}$ and $\phi_{\max}$, in a $\mathrm{sech}^2(x)$ refracting medium with $F_e/\eta=4$ and $g_0L=10$. The intermediate trajectory (heavy solid line) defines the path of a ray which exits the medium with angle $\phi_R \tanh(1)$, where $\phi_R \equiv \omega_{pe}/\omega$ is the refraction angle.

the intensity and coherence profiles are determined completely by the free modes. As F_e is increased or η decreased, successively new bound modes are born from the continuum. We have encountered difficulty in calculating the correlation function for parameters, i.e., F_e and η, in a small neighborhood of the condition described by Eq. (15). For example, the required high degree of cancellation between bound-mode and free-mode contributions to Eq. (13) is not obtained and the resulting correlation functions appear unphysical [13]. Possible explanations include insufficient numerical grid resolution and inappropriate use of Eq. (12) in employing the continuum limit near a free-mode resonance. Regardless of the exact nature of this problem, the parameter space in which such difficulties arise is comparatively small and straightforwardly avoided in practice. In cases where we care to examine the correlation function for such problematic parameters and avoid these difficulties, we can resort to the finite geometry method of Sec. III, which by design follows exactly each mode, bound or free, for any value of F_e and η.

The phenomenon of excess noise has a somewhat different manifestation for a smoothly varying profile compared to a square profile. In the case of a square profile our attention centered around removing excess intensity at large transverse distances $x \gg 1$ [5]. This is also of concern for the refracting medium, cf. Fig. 2(b), but we now often encounter in addition a robust increase in amplitude of the (normalized) bound eigenfunction $|v_n| \gg 1$ for $x < 1$, particularly for large F_e, which complicates further the implementation of the modal approach. Because of the strong coupling between the bound mode and its underlying free-mode resonance, cf. Fig. 2(b), this effect translates into large overlap integrals for the free modes and a correspondingly large *f-f* intensity. We find that a very significant degree of cancellation among the various intensity components, i.e., *b-b*, *f-f*, *b-f*, and *f-b*, occurs. For example, Figs. 6(a) and 6(b) display a total intensity profile and its various components, showing just how extreme the cancellation is in a refracting medium. Obviously, the modal approach in this case falls far short in providing a desired one-to-one correspondence between a physically intuitive laserlike mode and a particular mode of Eq. (2), owing to the strong cross correlation between modes. In this sense,

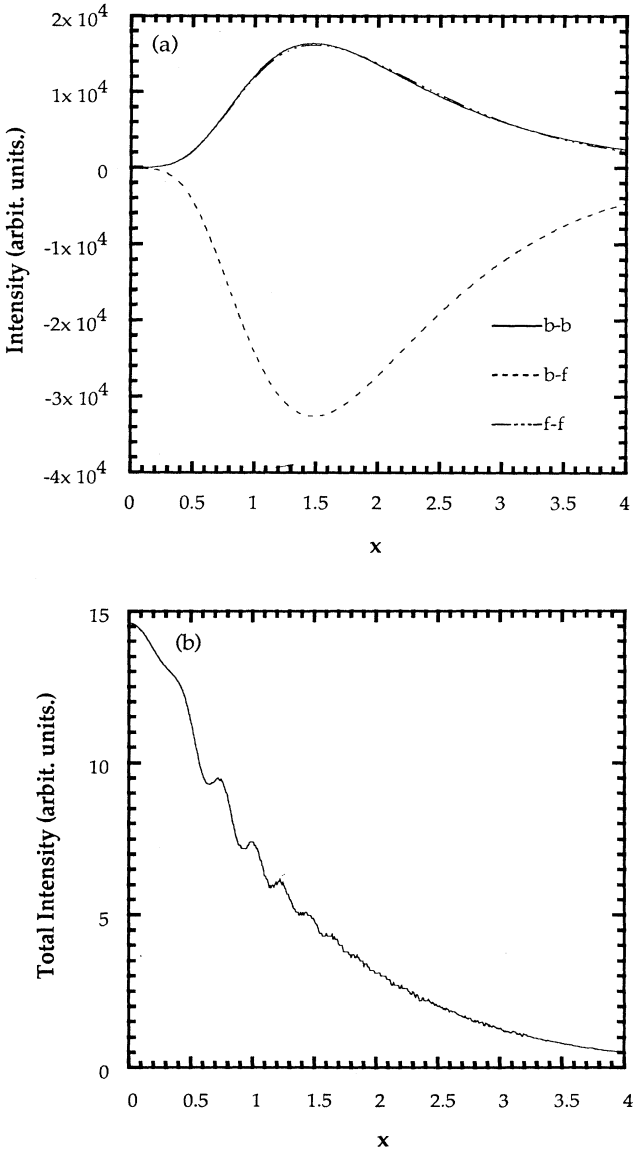

FIG. 6. (a) Bound-bound (*b-b*), bound-free ($b\text{-}f \equiv b\text{-}f + f\text{-}b$), and free-free (*f-f*) intensity contributions to Eq. (12) vs transverse distance x for $F_e=100$, $\eta=2.75$, and $g_0L=5$. (b) Total intensity is displayed; note the required amount of intensity cancellation by comparing the intensity scales in (a) and (b).

the individual modes of Eq. (2) should be viewed in most cases as strictly mathematical entities which only attain physical relevance after a spectrally complete summation over modes is performed, cf. Eq. (12). The exception occurs in the case of high gain discrimination where the fundamental bound mode principally determines the total intensity profile.

D. X-ray laser coherence parameter study

Fortunately, use of the modal approach in determining XRL coherence is not so severely constrained; only an effective cancellation within a (normalized) coherence length is required in practice. For most cases of interest this distance at which the coherence function μ drops from unity to sin(1) is of order unity or less and a numerical evaluation of Eq. (5) is still feasible.

We have undertaken a parameter study of coherence over a wide range of conditions which are relevant for current or planned experiments. The three fundamental parameters that we vary are g_0L, η, and the (horizontal) Fresnel number $F_x = F_e/g_0L$. The Fresnel number ($\propto a^2$) is quite variable owing to the freedom in selecting the laser half-width a. The density parameter is fixed by the lasing transition wave number k while the gain strength g_0 and plasma electron density depend on the hydrodynamics of the exploding plasma foil. The maximum (small-signal) gain-length product is typically fixed at 15–20 due to saturation effects.

In Fig. 7 we plot the normalized coherence length x_c versus g_0L for strong ($\eta=50$) and moderate ($\eta=10$) refraction for $F_x=20$. In both cases the coherence length scales as a power law for small g_0L with stronger scaling at higher g_0L. At higher g_0L a significant advantage in strong refraction is evident. In Figs. 8(a) and 8(b) we display the coherence length as a function of η for three values of the Fresnel number. A significant increase in coherence length with η is clear, particularly for $g_0L=15$. We note that relatively large coherence lengths are obtained for larger η and g_0L when F_x is less than about 40. Finally, Fig. 9 demonstrates how rapidly the coherence improves as the Fresnel number is decreased for two different g_0L values at $\eta=50$. We observe that x_c scales approximately as $1/F_x^2$ for small Fresnel number and large η, which is in strong contrast to the usual $1/F_x$ scaling for an incoherent source.

The criterion we choose to use in characterizing "good" coherence is that the near-field coherence length should exceed a transverse intensity scale length, so that

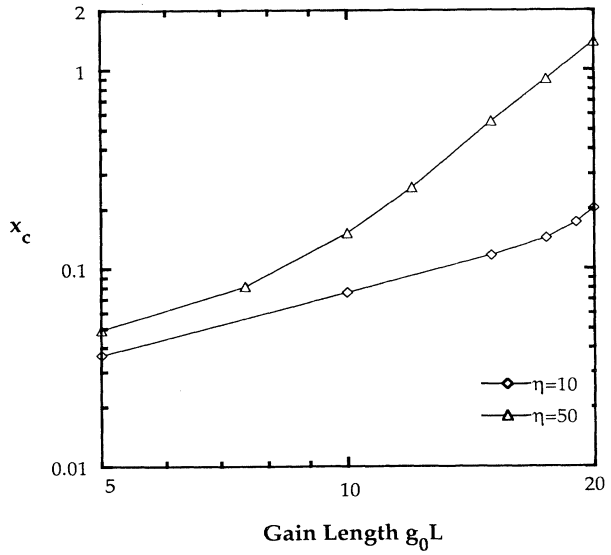

FIG. 7. Shown is the normalized coherence length x_c as a function of gain-length product g_0L for $F_x=20$ and $\eta=10$, 50.

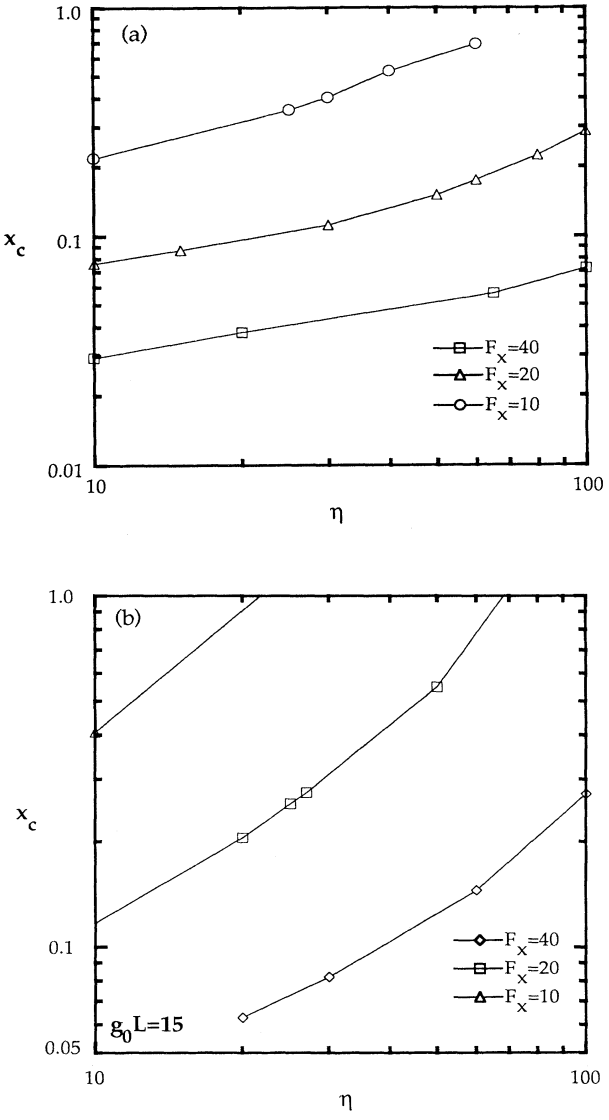

FIG. 8. Shown is the normalized coherence length x_c vs density parameter η for three values of the horizontal Fresnel number F_x when the gain-length product $g_0L=10$ (a) or 15 (b). In (a) the $F_x=10$ data extend only up to $\eta=60$ due to a resonance at $\eta=100$, cf. Eq. (14).

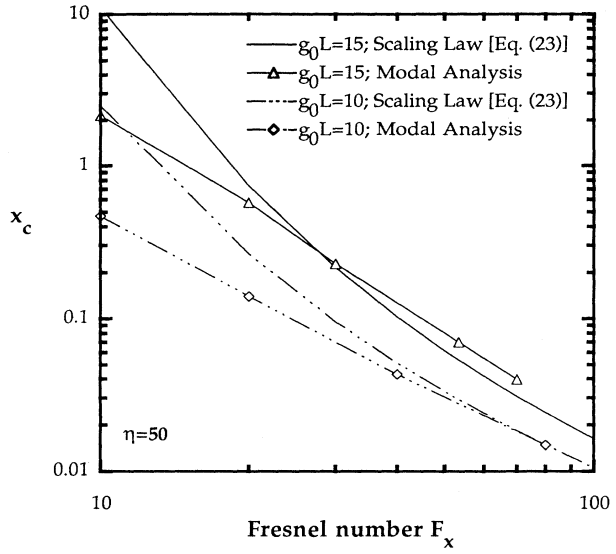

FIG. 9. Shown is the normalized modal coherence length x_c vs horizontal Fresnel number F_x for $\eta=50$ and gain-length product $g_0L=10$, 15. Also shown is the ray-optics scaling law [Eq. (23)] for coherence length divided by 2.8 to agree with the modal value of x_c at $F_x=80$, $g_0L=10$.

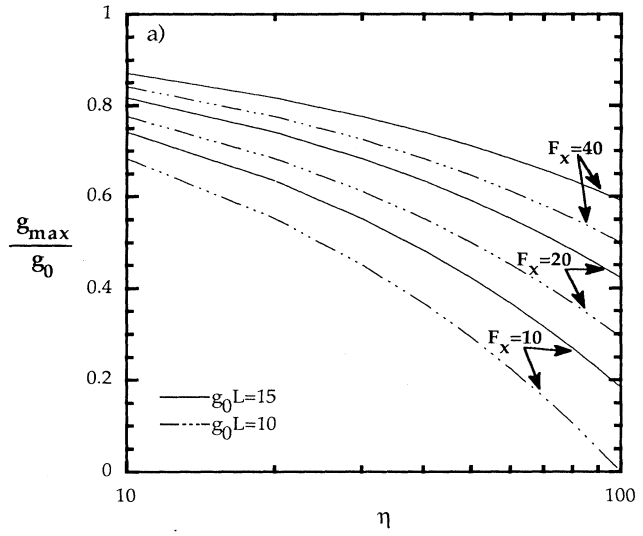

FIG. 10. Shown are the (fractional) maximum modal gains possible vs density parameter η for gain-length product $g_0L=10$ (dotted-dash line), $g_0L=15$ (solid line), and three values of Fresnel number F_x.

a significant fraction of the output is coherent. For the $\mathrm{sech}^2(x)$ profile, we can estimate an (unnormalized) intensity scale length L_I by calculating the transverse distance over which the intensity is reduced by $1/e$ from its on-axis value due to gain narrowing and refraction. For $F_e \gg \eta$, the intensity profile is strongly dominated by the lowest-order even-parity bound eigenfunction due to gain discrimination, giving $L_I = a\ \mathrm{sech}^{-1}\{1/\exp[(F_e/\eta)^{1/2}-1]^{-1}\}$. As we approach the strongly refracting regime ($F_e \to \eta$), the free modes begin to dominate the intensity profile and we must include all modes in order to determine x_I. In this manner, we are able to quantify the degree of transverse coherence.

At this point we can summarize very succinctly the indicated trend toward improved coherence: a decreasing *refraction* length $L_R \equiv a/\phi_R = L(F_x/g_0L\eta)^{1/2}$, or length along which a ray stays within the lasing medium before bending out, is associated with enhanced coherence because of stronger refractive defocusing. However, another important quantity to consider is the coherent energy output at the end of the laser. Unfortunately, the stronger refraction responsible for enhanced coherence may also cause a rapid deterioration of on-axis intensity. From Eq. (6) we note that the strongest growing bound mode ($n=0$) has the following reduced gain for $\eta \gg 1$:

$$\frac{g_{\max}}{g_0} = 1 - \left[\frac{\eta}{F_x g_0 L}\right]^{1/2}, \tag{16}$$

which agrees with the ray-optics treatments of XRL intensity in a parabolic medium [12,14]. In Fig. 10 we display this reduced gain versus η for several values of g_0L and F_x. For current XRL experiments with Ne-like Se at 206 Å, a minimum a of 200 μm with $\eta=100$ and $g_0L=15$ near saturation gives $F_x \approx 320$ and a gain reduced by only 10%. However, the associated coherence length is quite small, or less than 0.01. A direct approach toward improved coherence is to reduce a. For example, by narrowing a to 50 μm so that $F_x \approx 20$, the coherence length is greatly improved ($x_c \approx 0.5$), cf. Fig. 9, but the gain of the strongest mode is now reduced by 57%.

The decrease in maximum growth with increasing refraction does not completely describe the dependence of on-axis intensity on refraction. In particular, the overlap integrals B_{nm} entering Eq. (4) for the intensity tend to *increase* rapidly with refraction. The coherent power is obtained by integrating the intensity $(c/8\pi)\langle|E_\omega(\mathbf{r})|^2\rangle$ over both transverse directions, i.e., x and y, up to a respective coherence length. As described in Sec. II our basic physical model consists of a vertical gain profile which is nearly flat and with scale length b much larger than the horizontal (rounded) gain profile scale length a. Thus, optimal transverse coherence is associated with the horizontal direction. According to our model assumptions, the vertical coherence length is small compared to the vertical intensity scale length. Applying the van Cittert-Zernike theorem in the vertical direction gives a vertical coherence length $L_{cy} = b/F_y$, where $F_y = kb^2/L$ is the vertical Fresnel number. In addition, an implicit summation over the y transverse eigenfunctions in evaluating $(c/8\pi)\langle|E_\omega(\mathbf{r})|^2\rangle$ introduces an additional factor of F_y/π which simply corresponds to an estimate for the number of modes in the vertical dimension [15]. Thus, the vertical integration over intensity is trivially accomplished with use of the definition of C_1 below Eq. (4), and our calculation of coherent power effectively reduces to a one-dimensional transverse problem. Two additional considerations are the inclusion of gain narrowing in C_1 through the prescription $\Delta\omega \to \Delta\omega/\sqrt{g_0L}$, and a sensi-

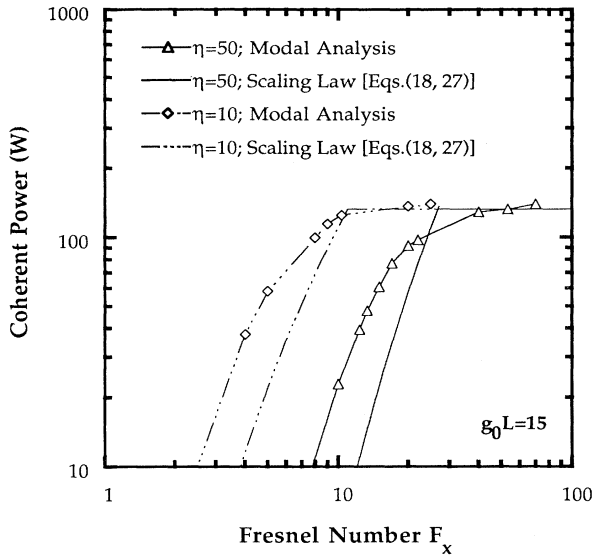

FIG. 11. Shown is the coherent power vs Fresnel number F_x for $g_0L=15$ and $\eta=10$, 50 in Ni-like Ta based on a modal analysis and a ray-optics scaling law [Eqs. (18) and (27)].

ble choice for $N_2/\Delta N:\approx 2$.

In Fig. 11 we display the coherent power in Ni-like Ta versus Fresnel number for $g_0L=15$, and $\eta=10$, 50. We find evidence for a critical Fresnel number ($F_x\approx 25$ for $\eta=50$) below which the coherent power sharply decreases as F_x is reduced. Below this value of Fresnel number, stronger refraction serves only to degrade the coherent power. Consequently, a reliance on increased refraction for improved coherence has its limits, and we may consider multipassing architectures with spatial filtering as a possible means of improving coherent output below this optimal regime.

V. SCALING LAW FOR COHERENCE BASED ON GEOMETRIC OPTICS

A. Introduction

Using the modal analysis, we have calculated the coherence properties of x-ray lasers for a broad range of parameters. In this section, we consider an alternate framework in order to understand the variations of coherence length and coherent power with input parameters, and to the results, particularly to larger Fresnel number F and smaller density parameter η, for which modal calculations are difficult. The framework is based on a geometric optics model, in which coherence is related to the angular distribution of radiation.

We review elements of the geometric optics treatment of x-ray laser propagation [12]. The radiation is characterized by the specific intensity I_ω defined as the amount of energy crossing a unit area per unit time, per unit solid angle, and per unit angular frequency. The specific intensity is generally a function of space, propagation direction, frequency, and time. The intensity discussed in the modal analysis, i.e., the electric-field correlation function evaluated at identical positions $\mathbf{r}_1=\mathbf{r}_2$ [see Eq. (4)], is equivalent to the angular integral of I_ω. The specific intensity is found by solving the radiative transfer equation along ray trajectories. The angular distribution is given by the specific intensity of the various rays passing through a given location. Ray trajectories, generally curved due to refraction, are determined from the eikonal equation [8]. The specific intensity characterization used here does not contain phase information, which can be included in more complete geometric optics treatments (see the second paragraph of Sec. V C and Ref. [16]). However, we believe that the angular distribution of the specific intensity implicitly contains sufficient information to estimate the coherence length as discussed in Sec. V C.

B. Incoherent disk-source model

In order to motivate a geometric optics formulation of coherence length, we discuss a simple incoherent disk-source model applied to a laser with constant gain and no refraction. We assume that spatially uncorrelated spontaneous emission occurs from a disk at one end of an elongated medium having half-width a, cross-sectional area A_s, and length L. The laser medium only acts to amplify the specific intensity according to a solution of the radiation transfer equation $I_\omega=S\exp[g_0L]$, where $S=(2h\omega^3/16\pi^4c^2)(N_2/\Delta N)$ is the spontaneous-emission source function, and we have assumed that the amplification is large ($\exp[g_0L]\gg 1$). The frequency dependence of the specific intensity is due to the variation of gain over a narrow line profile, which is due mainly to thermal motion of the lasing ions in x-ray lasers. Assuming that the phase of the electromagnetic waves propagates as in free space, we calculate the transverse coherence length at the output of the laser from the van Cittert-Zernike theorem [7–9]. For a rectangular-shaped source region, the coherence length (in dimensional units) is $L_c=1/[k(a/L)]$, as earlier introduced in Sec. II. Detailed wave optics calculations for nonrefracting ($\eta=0$) square profile lasers using the modal method give coherence lengths in good agreement with this simple formula [3,17].

The coherent output power is defined as the power passing through a specified coherence area A_c:

$$P_c=\int_{A_c} I_\omega d\omega\, d\Omega\, dx\, dy\ . \tag{17}$$

To find P_c, we add a second transverse dimension to the model as in Sec. IV. We denote this direction as the vertical or y direction and ascribe to it a characteristic half-width b. We define the coherence area as $A_c\equiv L_{cx}L_{cy}$, where L_{cx} and L_{cy} are the coherence lengths in the x and y directions, respectively. This definition of coherence area, in conjunction with the definition of L_c as the point at which the coherence function reaches ≈ 0.84, yields a very conservative measure of coherent power. A useful alternate definition of coherence area is discussed by

Goodman [7]: $A_{cG} \equiv \int |\mu(x,y)|dx\,dy$. Goodman shows that $A_{cG}=\lambda^2/\Omega_s$ is independent of the shape of the source, where Ω_s is the solid angle subtended by the source as viewed from the end of the laser. For a rectangular source of size $2a \times 2b$, $\Omega_s = 4ab/L^2$, and Goodman's coherence area is larger than ours by a factor of π^2. The number of modes in the system is on the order of $A_s/4A_c = F_x F_y$, where F_x and F_y are the Fresnel numbers in the x and y directions, respectively.

To evaluate P_c from Eq. (17), we first approximate the angular integral by assuming that I_ω is constant over Ω_s. We then integrate in frequency over the gain profile by the method of steepest descent, assuming $g_0 L \gg 1$. We then carry out the spatial integral for the limiting case in which the angle- and frequency-integrated intensity is approximately constant over A_c; we refer to this case as the partially coherent case. The result for P_c is

$$P_c \cong \Delta\omega_D \frac{S}{k^2} \frac{e^{g_0 L}}{\sqrt{g_0 L}} \frac{1}{\sqrt{\pi \ln 2}} . \tag{18}$$

The main determinant of P_c is the gain length $g_0 L$; the cross-sectional geometry has dropped out because of a cancellation of the angular factor in both L_c and the angle-integrated specific intensity. This result for P_c is shown in Sec. V D to hold generally in the incoherent case. This formula is valid until either a single mode is reached as $A_c \to A_s$, or the gain saturates, as discussed further in Secs. V D and V E.

C. Fundamental hypothesis for coherence length

As commonly noted in the literature [9,18,19], the factor a/L in the formula for the coherence length can be interpreted as the angle subtended by the source at the position where the coherence is measured. Similarly, the coherence area is related to the source solid angle. We now generalize this interpretation to lasers with arbitrary gain and refractive index variation, making the fundamental ansatz of replacing the factor a/L with the angular width of the specific intensity distribution at a particular output position of the laser $\Delta\phi$, as illustrated in Fig. 12. We thus write

$$L_c = \frac{1}{k\Delta\phi} . \tag{19}$$

Variations in gain and refractive index within the laser are assumed to affect the coherence only by altering $\Delta\phi$ from the simple geometric factor a/L. To find the coherence length we must calculate $\Delta\phi$ from the ray trajectories and integrated gain lengths along the rays. The coherent power is found from the angle and space integral of intensities along these same rays, as indicated in Fig. 12.

Before applying Eq. (19), we remark that the angular width hypothesis $a/L \to \Delta\phi$ is supported by several additional facts. One supporting argument is the observation that the specific intensity is directly proportional to the energy per mode (in a vacuum) [9,19], which suggests that the specific intensity is related to coherence power as indicated in Eq. (18). Another supporting fact is based on the derivation of the transverse coherence length of radiation from an incoherent planar source using optical path-length differences (see Ref. [9], pp. 552 and 553, and Ref. [18]). Consider the interference patterns created by radiation from two points on opposite sides of the source, passing through two slits. The radiation from the two points is assumed uncorrelated and thus the two interference patterns are independent. The interference patterns overlap when the slits are very close, and become significantly offset from each other when the slits are far apart. The slit separation at which the two interference patterns are offset by one half of a pattern wavelength is identified as the transverse coherence length. This separation is such that the second-order difference in optical path length along rays from the source points to the slits is approximately one half of the radiation wavelength. We have generalized this derivation to a working definition of coherence length and applied it to a laser with parabolic gain and density profiles. We have calculated the optical path-length differences from maximally separated (extreme) source points to two slits, including the effect of refractive index variation on both the trajectories and on the phase along rays, and the effect of gain variation in selecting the appropriate extreme source points. The result is a formula for the coherence length which is identical to that derived from the intensity angular width hypothesis [see Eq. (23) below].

D. Coherence length and power for sech^2 profiles

We now derive scaling laws for the coherence length and power for sech$^2(x)$ profiles. We generalize the solution for the specific intensity to account for ray-dependent gain $I_\omega = S \exp[\int g(s)ds]$, where s is the path length along a ray characterized by exit position and exit

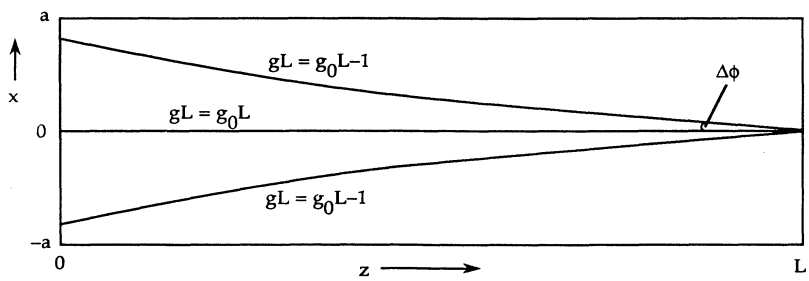

FIG. 12. Shown are the bounding ray trajectories used in calculating the normalized transverse coherence length [Eq. (23)].

angle. We have again assumed that the amplification is large. We calculate $\Delta\phi$ for radiation emerging from the center of the laser at $x=0$ since the intensity peaks at this position. To be definite, we take $\Delta\phi$ as the exit angle of the ray whose gain length is reduced by unity from the maximum gain-length ray. The specific intensity is thus reduced by $1/e$ from the maximum on-axis value. The implicit equation for this ray is

$$\int_0^{s_0} ds\, g(s) = g_0 L - 1 \ . \tag{20}$$

We call the ray satisfying Eq. (20) the bounding ray. The variation of gain along the bounding ray is included via the known transverse gain profile, i.e, the $\mathrm{sech}^2(x)$ function, and the ray trajectory found from the eikonal equation in the paraxial approximation [8]:

$$\frac{d^2x}{dz^2} = \frac{d\ln n(x)}{dx} \ , \tag{21}$$

where $n(x)=[1-\omega_{pe}^2/\omega^2]^{1/2}\approx[1-\phi_R^2\,\mathrm{sech}^2(x)]^{1/2}$ is the index of refraction. To determine $\Delta\phi$ we first solve Eq. (21) for all ray trajectories and then apply Eq. (20) to find the particular trajectory on which the intensity is reduced by $1/e$ at $z=L$ compared to the on-axis intensity. The exit angle of this particular ray is $\Delta\phi$. We can obtain an analytic result by making the approximation $(\Delta\phi/\phi_R)^2\sinh^2(L/L_R)\ll 1$, which turns out to be equivalent to approximating the $\mathrm{sech}^2(x)$ profile by a parabolic function. The result is

$$\Delta\phi = 2\phi_R \left\{ g_0 L_R \left[\sinh\left[\frac{2L}{L_R}\right] - \frac{2L}{L_R} \right] \right\}^{-1/2} \ , \tag{22}$$

where L_R is defined before Eq. (16). Substituting Eq. (22) for $\Delta\phi$ into Eq. (19), we have

$$x_c = \frac{L_c}{a} = \frac{1}{2F_x} \left[\frac{L}{L_R}\right]^{-3/2} \sqrt{g_0 L} \times \left[\sinh\left[2\frac{L}{L_R}\right] - 2\frac{L}{L_R} \right]^{1/2} \ . \tag{23}$$

In the nonrefractive limit ($L \ll L_R$), Eq. (23) reduces to $x_c=(g_0L/3)^{1/2}/F_x$, which is the usual square profile result now multiplied by a term proportional to $(g_0L)^{1/2}$. This latter factor describes an effective narrowing with gain length of the transverse region responsible for high output. In the strongly refracting limit ($L \gg L_R$),

$$x_c = \frac{1}{2\sqrt{2}F_x} \left[\frac{L}{L_R}\right]^{-3/2} \sqrt{g_0 L}\, e^{L/L_R} \ , \tag{24}$$

so that the coherence length grows approximately exponentially with length due to defocusing by refraction. The range of validity of Eq. (24) can be seen by considering the condition on $\Delta\phi/\phi_R$ above Eq. (22). For the strongly refracting limit ($L \gg L_R$) this condition can be expressed as $g_0 L_R \gg 2$, which still allows a broad and useful range of parameters. Experience with ray optics indicates that the inequalities need only be satisfied moderately in order for Eqs. (22) and (24) to remain quite accurate.

We have studied the sensitivity of Eq. (23) [through Eq. (20)] to an arbitrary number γ of e-folding lengths of specific intensity in defining $\Delta\phi$. We find a mild dependence on γ through the relation $x_c \to x_c/\sqrt{\gamma}$.

In Fig. 9 we compare the coherence length estimated with Eq. (23) to the modal results. The analytical result has been divided by a constant ($=2.8$) chosen to match the modal results at $\eta=50$, $F_x=80$, and $g_0L=10$. The need for this correction factor may be due to a difference in the shape of the coherence function for the $\mathrm{sech}^2(x)$ and parabolic profile and the choice of the $1/e$ intensity falloff for defining $\Delta\phi$. There also may be some systematic error in the modal analysis for large Fresnel numbers involving incomplete cancellation between free and bound modes. Nevertheless, the scaling law gives the correct order of magnitude and reproduces the variations of the coherence length quite well for large Fresnel numbers. For smaller Fresnel numbers, where only a few modes contribute to the intensity, the ray-optics description appears inaccurate. This is not surprising because the failure of ray optics is expected to occur for small Fresnel number [20]. We do not believe that the difference at small Fresnel number is a result of the parabolic approximation. It appears from Fig. 9 that a wave optics treatment such as the modal approach is necessary to reliably treat coherence for Fresnel numbers less than about 30 when $\eta > 50$, as in current experiments. For larger Fresnel numbers, the geometric optics description as embodied in Eq. (19) may be used to estimate coherence. A more accurate geometric optics treatment, which treats the imaginary and real parts of the index of refraction on an equal footing, may prove promising [16,21,22]. To estimate the coherent power we assume (nonrefracting) square gain and electron density profiles of width b in the y direction as discussed at the end of Sec. IV.

In each transverse direction two limiting cases exist: the partially coherent case, in which the scale length for the (angle-integrated) intensity (L_I) is larger than the coherence length (L_c), and the highly coherent case, in which the coherence length is larger than the intensity scale length. We assume the partially coherent case for the vertical direction ($L_{Iy} \gg L_{cy}$), while considering both cases for the horizontal direction x.

In the partially coherent case $L_{Ix} \gg L_{cx}$, we approximate P_c from Eq. (17) as

$$P_c \cong L_{cx} L_{cy} \Delta\Omega \int I_\omega d\omega \ . \tag{25}$$

Using $\Delta\Omega=[4b/L]\Delta\phi$, we readily find the same result for P_c as in Eq. (18) for the simple disk-source model without refraction or gain variation. The transverse geometry has again dropped out of the expression for coherent power. In the partially coherent case the coherent power scales quite strongly with gain length.

In the highly coherent limit ($L_{cx} \gg L_{Ix}$), Eq. (17) becomes

$$P_c \cong L_{Ix} L_{cy} \Delta\Omega \int I_\omega d\omega \ . \tag{26}$$

To obtain an analytic estimate, and in keeping with the approximation made in deriving Eq. (22), we use a parabolic profile to estimate the intensity scale length $L_{Ix}=a(2/g_0L_R)^{1/2}$, which is valid for $L\gg L_R$ and $g_0L_R>2$ (see Ref. [12]). Using Eq. (22) for $\Delta\phi$ and evaluating the frequency integral as in Eq. (18), we find from Eq. (26)

$$P_c\cong\omega\left[\frac{N_2}{\Delta N}\right]\frac{\hbar\Delta\omega_D}{\sqrt{g_0L}}\frac{\eta e^{g_0L}}{\left[\sinh\left[\frac{2L}{L_R}\right]-\frac{2L}{L_R}\right]}\left[\frac{2}{\pi^5\ln 2}\right]^{1/2}. \tag{27}$$

In Fig. 11 we have plotted the coherent power using Eqs. (18) and (27) in their respective limits. Comparison with the modal coherent power shows good agreement, particularly in the predicted location of the onset of declining coherent power from excessive refraction. The ray-optics results are systematically lower than the modal predictions at low Fresnel number due to an apparent underestimate of $\Delta\phi$; this feature is also evident in Fig. 9 for small Fresnel number.

The transition from partial to high coherence occurs when $L_{cx}=L_{Ix}$. This condition can be expressed in terms of a critical Fresnel number for high coherence F_c. In the case $L\gg L_R$ and $g_0L_R>2$, we evaluate F_c by equating the coherence length given in Eq. (24) with the intensity scale length $a(2/g_0L_R)^{1/2}$ discussed below Eq. (26), giving $F_c\equiv\eta g_0L/[\ln(4\eta)]^2$. This critical Fresnel number represents an optimal condition simply because a maximum coherence length is achieved without degraded coherent power. The optimal coherence criterion $F=F_c$, derived here by geometric optics methods, is identical to the criterion for good coherence derived from a wave optics analysis using only bound modes [3].

E. Maximum coherent power at saturation

For practical applications such as x-ray holography, the coherent energy output of a laser is important. Using Eqs. (18) and (27), we can estimate the coherent power as plotted in Fig. 11. Given a small-signal gain coefficient (g_0), we want the end of the laser to barely coincide with the onset of gain saturation, since the coherent power will then grow exponentially with gain length along the entire length of the laser. For a 45-Å nickel-like tantalum laser with standard parameters of $a\approx b\approx 75$ μm and $\eta\approx 150$ (see Table I), we estimate a maximum saturation gain length of about 20 and coherent energy outputs on the order of one μJ in 100 psec. Such output is not large enough for holographic applications in biology and larger gain-length products are therefore desired.

To create a laser with large gain length and increased coherent output, we need to consider some details of gain saturation. By gain saturation we mean the reduction of the gain coefficient caused by stimulated emission transferring significant population from the upper state of the laser to the lower state. This happens at large gain length when the amplified radiation field has become so strong that the stimulated emission rate is comparable to other rates. When the saturation gain length is exceeded, the growth of intensity becomes linear rather than exponential. To extract the maximum coherent energy, we propose configuring the laser such that the coherence fraction approaches unity at saturation. This avoids saturating the laser with unwanted incoherent radiation. As we show below, the increased coherence length caused by refraction is accompanied by a filtering of such unwanted radiation. Therefore, the saturation gain length is increased and more coherent power can be extracted.

To determine the saturation gain length, we introduce a line mean intensity J, defined as the average of the radiation intensity over angle and frequency, but weighted by the line profile function $\psi(\omega)$:

$$J\equiv\frac{1}{4\pi}\int I_\omega\psi(\omega)d\Omega\,d\omega\ , \tag{28}$$

where the line profile obeys the normalization $\int d\omega\,\psi(\omega)=1$. The stimulated emission rate is $R_s=16\pi^4JA_E(c^2/2h\omega^3)$, where A_E is the spontaneous-emission rate (or "Einstein A coefficient"). We evaluate Eq. (28) using the ray solution for I_ω, the steepest-descent approximation for the frequency integral, and a solid angle factor for the angular integral

$$J=\left[\frac{S}{4\pi}\right]e^{G_{\max}}\Delta\Omega/\sqrt{G_{\max}}\ , \tag{29}$$

where $G_{\max}$ is the maximum gain length as a function of angle at a particular exit position, and S is the source function. The saturation mean intensity is estimated by equating the stimulated emission rate to the total exit rate E_{out} from the upper laser state excluding stimulated processes: $J_{\text{sat}}=(2h\omega^3/16\pi^4c^2)E_{\text{out}}/A_E$. The emission rate E_{out} generally includes collisional rates in addition to the spontaneous rate A_E.

We now look for the maximum coherent power at saturation, and the laser configuration to achieve such power. For a square profile, the optimuum condition, i.e., $L_{Ix}\approx L_{cx}$, is $F=1$, since $L_{Ix}\approx a$ and $L_{cx}\approx a/F$. Using $\Delta\Omega=4ab/L^2$, the saturation condition reads

$$\frac{\exp(G_{\text{sat}})}{G_{\text{sat}}^{3/2}}=\frac{k}{g_0}\frac{1}{\sqrt{F_y}}\frac{\pi E_{\text{out}}}{A_E\tilde{S}}\ , \tag{30}$$

where $F_y=1$ corresponds to maximum coherence, G_{sat} is the saturation gain-length product, and $\tilde{S}=[1-g_2N_1/g_1N_2]^{-1}$ is a dimensionless source.

For the parabolic profile, we solve two simultaneous equations: the optimal coherence condition, i.e., $F=F_c$, and the saturation condition $J=J_{\text{sat}}$. From Eqs. (22) and (29), we find the following implicit equation for G_{sat}:

$$\frac{e^{G_{\text{sat}}}}{(G_{\text{sat}}^{3/2}-\zeta G_{\text{sat}}^{1/2})}=\frac{k}{g_{\text{obs}}}\frac{1}{\sqrt{F_y\eta}}\left[\frac{\pi}{2}\frac{E}{A\tilde{S}}\right]\times\left\{\frac{\sinh[2\zeta]}{\zeta}-2\right\}^{1/2}, \tag{31}$$

where $\zeta=\ln[4\eta]$, and g_{obs} is the *observed* gain strength of

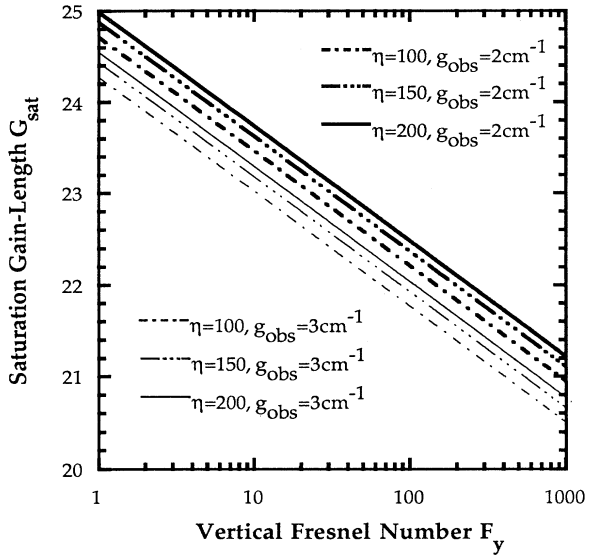

FIG. 13. Shown is the optimal saturation gain-length product G_{sat} vs vertical Fresnel number F_y for $\eta=100$, 150, 200, and observed gain $g_{obs}=2$, 3 cm^{-1} in Ni-like Ta.

the lasing medium after allowing for refraction through Eq. (16). In Fig. 13 we display the solution of Eq. (31) for G_{sat} in Ni-like Ta for the $4d^{3/2}\rightarrow 4p^{1/2}$ transition at 45 Å for several values of η and g_{obs} as the vertical Fresnel number F_y is varied. We have determined the quantity $E_{out}/A_E \approx 9.1$ based on simulations of a 40% Ni-like Ta x-ray lasing plasma with an electron (ion) temperature of 800 (430) eV and electron density $n_e=2\times10^{21}$ cm^{-3} [23]. We find that gain-length products up to $G_{sat}=25$ are permitted in the optimal case indicated ($F_y=1$, $g_{obs}=2$ cm^{-1}, $\eta=200$), as compared with $G_{sat}=23$ for the square profile, cf. Eq. (30). For current experimental conditions with $b\approx75$ μm, $F_y\approx100$, $g_{obs}\approx3$ cm^{-1}, and $\eta\approx150$, the maximum gain-length product is about 22. The corresponding coherent output energy is now on the order of 10 μJ in 100 psec, which falls short by nearly two orders of magnitude if we demand a resolution of 300 Å. Further improvement is possible if we legislate that the gain profile be strongly refracting in the vertical direction instead of squarelike, as we have assumed throughout this work. We thus require that F_y also satisfy the optimum condition $F=\eta g_0 L/[\ln(4\eta)]^2$, giving $a=b$. After making the replacement $\Delta\Omega\approx(2\Delta\phi)^2$ in Eq. (29) and repeating the procedure leading to Eq. (31), we find that $G_{sat}\approx26$ for $g_{obs}\approx2$ cm^{-1} and $\eta\approx150$. The physical characteristics of such an optimized Ni-like Ta laser are an output of nearly 0.5 mJ in 100 psec, a length of 13 cm and half-width of about 100 μm, and a coherence length of about 70 μm. This optimized coherent energy output now compares favorably with calculated requirements for coherent energy generation in holographic imaging studies of biological specimens at a useful resolution of 300 Å [2]. However, the operation of a single-stage amplifier at such an optimum level of performance necessary for holographic studies may prove unrealistic. Thus, a multistage or multipass architecture with spatial filtering should be considered as a practical alternative to an optimized single-stage x-ray laser.

VI. SUMMARY

Theoretical modeling of transverse coherence in XRL's is of current interest because of ongoing experimental efforts to study and optimize coherence for eventual holographic applications. As a further step in understanding the basic properties of transverse coherence, we have advanced the modal approach as a sensible alternative to wave optics simulations and propagator methods [24,16,25]. In this paper, we have extended our previous work on transverse square profiles and considered the importance of refraction in smoothly varying media on transverse coherence. Although a smooth profile is found to render the modal approach awkward to implement, we have succeeded in determining the degree of coherence for a wide range of parameters that is experimentally relevant. We have found that current XRL designs are not expected to be very coherent, as confirmed by recent measurements [26]. We have also shown that refraction helps a great deal in improving the coherence length, but only up to a certain point after which the coherent energy output rapidly drops. For the idealized profiles considered, we have identified an optimal operating range for a single-stage laser to achieve high coherent power.

Some unexplored phenomena may adversely affect coherence. For example, x-ray refraction by density fluctuations or driver-induced nonuniformities in single stage XRL's are suggested topics of future study. Use of multistage or multipass architectures may prove helpful toward relaxing the strict operating conditions associated with our optimized single-stage x-ray laser design.

ACKNOWLEDGMENTS

We are pleased to acknowledge stimulating discussions with Mike Feit, Brian MacGowan, Steve Maxon, Ricky Ratowsky, Mordy Rosen, Luis DaSilva, Jim Trebes, and Ed Williams. In addition, we thank Mike Feit and Joe Fleck for allowing us the use of WAVE for comparison with our modal analysis. This work was performed under the auspices of the U.S. Department of Energy by the Lawrence Livermore National Laboratory under Contract No. W-7405-ENG-48.

[1] M. D. Rosen *et al.*, Phys. Rev. Lett. **54**, 106 (1985); D. L. Matthews *et al.*, *ibid.* **54**, 110 (1985); B. J. MacGowan *et al.*, *ibid.* **65**, 420 (1990); R. C. Elton, *X-Ray Lasers* (Academic, San Diego, 1990).

[2] R. A. London, M. D. Rosen, and J. E. Trebes, Appl. Opt. **28**, 3397 (1989).

[3] R. A. London, M. Strauss, and M. D. Rosen, Phys. Rev. Lett. **65**, 563 (1990).

[4] K. Petermann, IEEE J. Quantum Electron. **QE-15**, 566 (1979); H. A. Haus and S. Kawakami, *ibid.* **QE-21**, 63 (1985); C. H. Henry, J. Lightwave Technol. **LT-4**, 288 (1986); A. E. Siegman, Phys. Rev. A **39**, 1253 (1989); **39**, 1264 (1989); J.-L. Doumont, P. L. Mussche, and A. E. Siegman, IEEE J. Quantum Electron. **QE-25**, 1960 (1989); P. L. Musche and A. E. Siegman, in *Laser Noise,* edited by R. Roy (SPIE, Boston, 1990), pp. 153–163; P. W. Milonni, *ibid.* pp. 164–171; I. H. Deutsch, J. D. Garrison, and E. M. Wright, J. Opt. Soc. Am. B **8**, 1244 (1991); S. J. Kuo, D. T. Smithey, and M. G. Raymer, Phys. Rev. Lett. **66**, 2605 (1991).

[5] P. Amendt, R. A. London, and M. Strauss, Phys. Rev. A **44**, 7478 (1991).

[6] The prefactor of 2 in C_1 arises from allowing a *two*-dimensional sense of transverse polarization instead of a one-dimensional prescription as adopted in Refs. [3,5].

[7] J. W. Goodman, *Statistical Optics* (Wiley-Interscience, New York, 1985).

[8] M. Born and E. Wolf, *Principles of Optics* (Pergamon, Oxford, 1980).

[9] P. W. Milonni and J. H. Eberly, *Lasers* (Wiley-Interscience, New York, 1988).

[10] L. D. Landau and E. M. Lifshitz, *Quantum Mechanics* (Pergamon, Oxford, 1977); I. I. Gol'dman and V. D. Krivchenkov, *Problems in Quantum Mechanics* (Pergamon, Frankfurt, 1961).

[11] By resonancce between free and bound modes, we specifically mean a coincidence between the real parts of E and E_n but not necessarily between the imaginary parts of E and E_n.

[12] R. A. London, Phys. Fluids **31**, 184 (1988).

[13] By a required high degree of cancellation, we specifically mean that the intensity contribution from a marginally bound mode and neighboring resonant free modes to the total intensity $I_{\rm tot}=I_{b\text{-}b}+I_{f\text{-}f}+I_{b\text{-}f}+I_{f\text{-}b}$ should nearly cancel, i.e., $I_{b\text{-}b}\approx I_{f\text{-}f}\approx -(I_{b\text{-}f}+I_{f\text{-}b})/2$. See Ref. [5] for a thorough discussion of local intensity cancellation for a square transverse profile.

[14] E. E. Fill, Opt. Commun. **67**, 441 (1988).

[15] Some ambiguity is found in the literature regarding a precise definition of Fresnel number. This ambiguity carries over directly to any attempt at estimating the number of transverse modes in a system. To resolve this dilemma we have considered a square profile model for the transverse gain and density profiles and computed the effective number of modes as compared with a vertical Fresnel number, which we define as $F_y=kb^2/L$. We numerically find that $0.3F_y$ approximates the number of transverse modes in the system when $\eta=0$. We have also analytically compared the angle-averaged energy flux from a ray-optics treatment in the absence of refraction with a modal estimate to find more precisely that the number of modes is given by F_y/π.

[16] G. Hazak and A. Bar-Shalom, Phys. Rev. A **38**, 1300 (1988).

[17] R. A London, P. Amendt, M. Strauss, M. D. Rosen, M. D. Feit, and J. A. Fleck, in *X-Ray Lasers 1990,* Proceedings of the Second International Colloquium on X-Ray Lasers, York, 1990), edited by G. J. Tallents (Institute of Physics, Bristol, England, 1990).

[18] S. G. Lipson and H. Lipson, *Optical Physics,* 2nd ed. (Cambridge University Press, Cambridge, England, 1981), pp. 239 and 240.

[19] Z. Karny, S. Lavi, and O. Kafri, Opt. Lett. **8**, 409 (1983).

[20] A. W. Snyder and J. D. Love, *Optical Waveguide Theory* (Chapman and Hall, London, 1983).

[21] R. Ratowsky (private communication).

[22] O. Zahavi, Z. Zinamon, and G. Hazak, Weizmann Institute of Science Report No. 4 (1992) (unpublished).

[23] S. Maxon (private communication).

[24] M. Feit and J. Fleck, J. Opt. Soc. Am. B **7**, 2048 (1990).

[25] G. Hazak and A. Bar-Shalom, Phys. Rev. A **40**, 7055 (1989).

[26] J. E. Trebes *et al.*, Phys. Rev. Lett. **68**, 588 (1992).

[27] B. J. MacGowan (private communication).